CALPHAD: Computer Coupling of Phase Diagrams and Thermochemistry 51 (2015) 224–232

Contents lists available at ScienceDirect

CALPHAD: Computer Coupling of Phase Diagrams and Thermochemistry

journal homepage: www.elsevier.com/locate/calphad

Thermodynamic assessment of the Al–Cu–Zn system, part I: Cu–Zn binary system

Song-Mao Liang [a], Hsien-Ming Hsiao [a,b], Rainer Schmid-Fetzer [a,*]

[a] Institute of Metallurgy, Clausthal University of Technology, D-38678 Clausthal-Zellerfeld, Germany
[b] Department of Materials Science and Engineering, National Taiwan University of Science and Technology, Taipei, Taiwan, ROC

ARTICLE INFO

Article history:
Received 21 August 2015
Received in revised form
28 September 2015
Accepted 29 September 2015

Keywords:
Phase equilibria
Thermodynamics
Calphad assessment
Cu–Zn system

ABSTRACT

The thermodynamic description of the Cu–Zn system is reassessed based on all original experimental data. Previous work on that subject is critically analyzed and the need for improvement is worked out. Tracing back to the original experimental data, the δ phase is acknowledged as hexagonal structure and thus modeled as a separate phase from the Bcc phase. An improved quantitative description of original experimental phase equilibrium and thermodynamic data for Zn-rich alloys is achieved without sacrificing the quality of description in the full composition range. The new γ phase model reflects the crystal structure and facilitates extension to ternary systems. The earlier suggested temperature dependence of the enthalpy of mixing in the liquid phase is shown to be deduced from derived data of vapor pressure and chemical potential in a narrow temperature range and is, thus, disapproved.

1. Introduction

Computational thermodynamics can provide guidelines for the exploitation of Zn–Al–Cu alloys, which are widely used in automotive components [1] and promising Pb-free solders [2]. A reliable thermodynamic description of the Cu–Zn system, especially in Zn-rich corner, is crucial to the reliability of the multi-component Zn alloy thermodynamic databases. Moreover, the Cu–Zn binary system is essential for Cu alloy and Al alloy thermodynamic databases, in which Cu and Zn are key elements.

Several thermodynamic descriptions of the Cu–Zn system are available in the literature [3–9]. Spencer [3] published the first one in 1986. Later Kowalski and Spencer [4] carried out a full thermodynamic evaluation of excellent quality and the calculated phase diagram is very close to the experimentally assessed phase diagram [10] except for the very Zn-rich corner. This thermodynamic description was accepted in the public COST507 database [5], but in the COST507 version it is modified by introducing a so-called HCP_Zn phase to differentiate the two hexagonal forms of Zn. This modification in COST 507 may be seen as deterioration since it produces artifacts and inconsistency in Mg–Zn and Cd–Mg based systems as shown by Schmid-Fetzer and Hallstedt [11]. Based on the proper original work of Kowalski and Spencer [4], Liang and Chang [6] simplified the γ-phase description from a four-sublattice to a single-sublattice model in order to facilitate the description of complete solid solubility of γ phase in the ternary Al–Cu–Zn system. David et al. [7] revised the thermodynamic description of Ref. [4] based on their own electromotive force (EMF) measurements on Zn-rich alloys. They improved the Zn-rich corner description from Ref. [4] but sacrificed the agreement of the other part of the phase diagram, especially at the β and γ phase boundaries [7]. Gierlotka and Chen [8] only changed the parameters of Bcc phase and liquid phase from Ref. [5] and provided two sets of thermodynamic descriptions by considering or disregarding the β/β′ disorder–order transition. They also introduced temperature dependence for the enthalpy of mixing of the liquid phase based only on the derived experimental enthalpy data, which is not reasonable as will be discussed later. Wang et al. [9] also based their description on COST507 [5] and only changed the model of γ phase to be (Zn)4(Cu,Zn)1(Cu,Zn)8 in an attempt to be combined with the γ phase in Al–Cu system which was modeled as (Al)4(Al,Cu)1(Cu)8 in COST507 [12]; however, no publication on the Al–Cu–Zn ternary description could be found by that group of authors [9]. It is emphasized that the model (Al)4(Al,Cu)1(Cu)8 for γ in the Al–Cu system [12] was only used to constrain the composition range of the γ phase and did not consider any crystal structure information. Wang et al. [9], similar to Ref. [8], also used the derived enthalpy data to fabricate a temperature dependence for the enthalpy of mixing of the liquid phase. It is emphasized that, after carefully evaluating all the previous thermodynamic descriptions, we found that none of the thermodynamic descriptions [5–9] published after Ref. [4] could be considered superior to that basic one [4] for describing the Cu–Zn binary system in the

* Corresponding author.
E-mail addresses: songmao.liang@tu-clausthal.de (S.-M. Liang), hmhsiao@iner.gov.tw (H.-M. Hsiao), schmid-fetzer@tu-clausthal.de (R. Schmid-Fetzer).

http://dx.doi.org/10.1016/j.calphad.2015.09.010
0364-5916/

complete composition range.

However, when applying the thermodynamic description by Ref. [4] to Zn-rich alloys and also when aiming at an extension to the Al–Cu–Zn ternary system there are three main problems: (i) for Zn-rich alloys the discrepancy to experimental data is significant, (ii) the δ phase should be modeled as a separate phase because it is not of Bcc structure, and (iii) the four sub-lattice model for the γ phase needs to be simplified. It is the purpose of this work to evaluate all the original experimental data and carry out a full thermodynamic reassessment of the Cu–Zn system to solve these three problems. This is considered as foundation for the comprehensive thermodynamic description of the ternary Al–Cu–Zn system worked out in this context.

2. Critical review of experimental literature data

2.1. Crystal structure of solid phases

Table 1 compiles the crystal structure information of all solid phases. For convenience the phase names in the first column are the same as used in Refs. [4,10]. The crystal structures assessed in Ref. [10] are accepted, except for the δ phase. The δ phase information provided in Table 2 of Ref. [10] is probably a typo; it should be referred to the ε phase which is the subject of the cited studies [13,14]. Thus, the crystal structure of δ was not included in that table of solid phases even though the δ phase was discussed in the text [10]. The crystal structure of the δ phase was first investigated by Schubert and Wall [15] and reported as cubic structure, the main diffraction lines could be indexed according to the CsCl (B2) cell with lattice parameter $a=301$ pm. Later work by the same first author together with Lenz [16] evidenced that the δ phase is hexagonal, with space group $C^1_{3h}P\bar{6}$, lattice parameters $a=427.5$ pm, $c=259.0$ pm, and with probably statistic distribution of atoms and vacancies. Thus Lenz and Schubert [16] clearly corrected their previously determined cubic structure [15]. This gives rise to one of the main distinctions of the present work to all previous thermodynamic descriptions [3,4,7–9], in which both the δ phase and the β phase are modeled as the same phase Bcc, as will be discussed later.

Table 1
Solid phases in the Cu–Zn binary system.

Phase name/temperature range (°C)[a]	Pearson symbol/*space group*/ prototype[b]	Model in Refs. [4,7,8[c]]	Model [this work]	Phase name in tdb-file [this work]
α, (Cu) ≤ 1084.62	cF4 *Fm-3m* Cu	$(Cu,Zn)_1$	$(Cu,Zn)_1$	Fcc
η, (Zn) ≤ 425	hP2 *P6$_3$/mmc* Mg	$(Cu,Zn)_1$	$(Cu,Zn)_1$	Hcp
β 903–452	cI2 *Im-3m* W	$(Cu,Zn)_1$	$(Cu,Zn)_1$	Bcc
β′ ≤ 462	cP2 *Pm-3m* CsCl	$(Cu,Zn)_{0.5}$ $(Cu,Zn)_{0.5}$	$(Cu,Zn)_{0.5}$ $(Cu,Zn)_{0.5}$	Bcc_B2
γ ≤ 834	cI52 *I-43m* Cu_5Zn_8	$(Cu,Zn)_4$ $(Cu,Zn)_4$ $(Cu)_6$ $(Zn)_{12}$	$(Cu)_4$ $(Cu,Zn)_6$ $(Cu,Zn)_{16}$	Gamma
δ 701–560	hP3 $C^1_{3h}P\bar{6}$ (*P-6*) $CuZn_3$(h)	$(Cu,Zn)_1$	$(Cu,Zn)_1$	Delta[d]
ε ≤ 598	hP2 *P6$_3$/mmc* Mg	$(Cu,Zn)_1$	$(Cu,Zn)_1$	Eps

[a] The phase names are the same as in Refs. [4,10]; the temperature range is from the calculated results in this work.

[b] Crystal structure data are from Ref. [10] except for the δ phase, which is from Ref. [16]. Assignment of prototype Mg for the ε phase is from Refs. [13,14]. See text for details.

[c] In Ref. [8] the β and β′ phases are modeled as two separate phases both with $(Cu,Zn)_1$ model.

[d] Phase description (and name in tdb) Bcc used for δ in Ref. [4] but described as separate phase Delta in this work.

2.2. Thermodynamic data

All the original experimental work on the thermodynamic properties of Cu–Zn binary system have been examined carefully and collected in Table 2 [7,17–38]. All thermodynamic property data have been used for thermodynamic optimization from their original values, rather than the derived data. A typical case of derived data is an integral enthalpy obtained from the temperature dependence of experimental vapor pressure or electromotive force (EMF) data; these direct data are compiled in Table 2, denoted as chemical potential data of Zn, μ_{Zn}, but not the derived enthalpy data. The enthalpy of mixing of the Cu–Zn liquid phase, $\Delta_m^{Liquid}H$, was only measured directly by Parameswaran and Healy [17] and Turchanin [18] using the calorimetry method. Samson-Himmelstjema [19] calculated the liquid property at 1000 °C based on their measured enthalpy values of the solid phases at 20 °C. Other reported enthalpy of mixing values were derived from the measured vapor pressure [25,29,32] and EMF data [31] and excluded from the compilation of original experimental data in Table 2.

2.3. Phase equilibrium data

Miodownik [10] evaluated about 100 references published from 1911 to 1989 in his excellent critical assessment of the Cu–Zn phase equilibria. In order to keep the present work concise, we accepted the assessed phase diagram [10] as experimental phase diagram basis for comparison. The original experimental phase equilibrium data and their references [39–48] are only given for the Zn-rich corner, where more detailed comparison of the refined present thermodynamic description of the Cu–Zn system with this earlier and also more recent work published in 2003 [7] is required.

3. Thermodynamic modeling

3.1. Pure elements

The Gibbs energy function, $G_i^{0,\varphi}(T) = G_i^{\varphi}(T) - H_i^{SER}$, of the pure element (i) (i=Cu and Zn), in any phase ϕ is described by an equation of the following form:

$$G_i^{0,\varphi}(T) = a + b{\cdot}T + c{\cdot}T{\cdot}\ln T + d{\cdot}T^2 + e{\cdot}T^3 + f{\cdot}T^{-1} + g{\cdot}T^7 + h{\cdot}T^{-9} \quad (1)$$

where H_i^{SER} is the molar enthalpy of the element (i) at 298.15 K and 1 bar in its standard element reference (SER) state, which is fcc for Cu and hcp for Zn. T is the absolute temperature. The "^{0}" in $G_i^{0,\varphi}(T)$ defines the so-called SER-reference state, which is, thus,

Table 2
Summary of original experimental work on thermodynamic properties of the binary Cu–Zn system.

Quantity measured	Method	Temperature (°C)	Composition range (at% Zn)	Reference
$\Delta_m^{Liquid}H$	Calorimetry	1127	5–85	[17]
	Adiabatic calorimeter	1100	10–40	[18]
	Calorimetry	1000 (Calculate from 20 °C)	0–100	[19]
$\Delta_f^{solid}H$	Calorimetry	300, 400	26–86.5	[20]
	Calorimetry	300	10–35	[21]
	Calorimetry	90	39–98	[22]
	Calorimetry	25	7–37	[23]
	Calorimetry	20	12–88	[19]
	Calorimetry	20	11.2–87.8	[24]
μ_{Zn}^{Liquid}	Boiling point method	1150	18–90	[25]
	Vapor pressure technique	1100, 1150	1–8	[26]
	Vapor pressure technique	1100	1–10	[27]
	Vapor pressure technique	850–1200	5–92	[28]
	Vapor pressure technique	927	8.1–85.3	[29]
	Vapor pressure technique	796–1030	32.9–79.2	[30]
	EMF	800–900	45–90	[31]
	Vapor pressure technique	700–850	42.8–79.8	[32]
	EMF	627	80–92	[33]
	EMF	395–558	90–98	[7]
μ_{Zn}^{solid}	Vapor pressure technique	790	1–10	[34]
	Vapor pressure technique	727	37.3–45.3	[35]
	Vapor pressure technique	727	2.1–34.1	[36]
	Atomic Adsorption method	500	5–35	[37]
	EMF	400, 500	44.4–84.3	[38]
	EMF	395–558	90–98	[7]

transferred to all phases in the subsequent equations in a simple way without using any H_i^{SER}again. The Gibbs energy functions for Cu and Zn are taken from the SGTE (Scientific Group Thermodata Europe) compilation by Dinsdale [49].

3.2. Substitutional solution phases

The Gibbs energies for liquid, α (Fcc), β (Bcc), δ, ε, and η (Hcp) phases are described in the substitutional solution model as follows:

$$G^{\varphi} = \sum_i x_i \cdot G_i^{0,\varphi} + RT\sum_i x_i \ln x_i + \sum_{i,j>i} x_i \cdot x_j \cdot \sum_{\nu} L_{i,j}^{\nu,\varphi} \cdot (x_i - x_j)^{\nu} \quad (2)$$

where x_i (x_j) represents the mole fraction of elements (i) (j), with (i) (j)=Cu and Zn. R is the gas constant (R=8.3145 J/mol K) and $L_{i,j}^{\nu,\varphi}$ is the Redlich–Kister parameter representing the interaction of order ν between elements (i) and (j) in phase ϕ. This interaction parameter, $L_{i,j}^{\nu,\varphi}$, may be linearly temperature dependent and is usually expressed as $L_{i,j}^{\nu,\varphi} = A_{i,j}^{\nu,\varphi} + B_{i,j}^{\nu,\varphi} \cdot T$. Interaction parameters beyond order ν=2 are generally not considered reasonable.

3.2.1. The δ phase

In all previous thermodynamic descriptions [3,4,7–9], both the δ phase and the β phase are modeled as the same phase Bcc. In Ref. [4] it is claimed that "the two Bcc phases, δ and β, are both of the same W structure type" and two Refs. [50,51] were given. In Ref. [50] two Cu–Zn compounds $CuZn_2$ and Cu_5Zn_8 are collected with the following data: for $CuZn_2$ it is hP3, space group of P-6, source Ref. [16]; for Cu_5Zn_8 it is cI52, space group I-43m, source Ref. [52]. There are, however, only two lines printed for the entire "Cu–Zn system" in Ref. [51]: "β: A2, β′: B2, γ: $D8_2$, δ: B2, ε: A3. The Cu–Zn phase diagram is redrawn from [Metals]". Possibly this information "δ: B2" in Ref. [51] was taken from the earliest work [15] without considering the correction made in 1971 by Lenz and Schubert [16] for the $CuZn_3$(h) phase δ. Probably Kowalski and Spencer [4] accepted the δ as B2 from [51] and simplified it further to the disordered A2 (Bcc, cI2, W) structure. Thus, in their thermodynamic description [4] δ is modeled as the same phase as β, but, interestingly, not as the ordered β′ (B2) phase. We failed to find any other literature which can support the δ phase to exhibit Bcc structure of prototype W. Therefore, in this work, the δ phase is modeled as a separate phase from Bcc phase due to its different hexagonal crystal structure.

3.2.2. The ε and η phases

Even though the terminal η phase (Zn) and the distinct ε phase are both of the Hcp (A3) structure they were modeled as separate phases in Ref. [4] because unrealistic interaction parameters would have been required to model the η+ε two-phase region as a spinodal miscibility gap. We agree with that description of η (Zn) as Hcp (A3) and ε as distinct intermetallic phase but not with the choice of the end member parameter of ε at pure Cu, set as $G_{Cu}^{0,fcc}+1$J by Ref. [4]; because of the Hcp crystal structure it should be better set equal to $G_{Cu}^{0,hcp}$. We agree with the choice for the other metastable end point of the ε phase at pure Zn [4], set equal to $G_{Zn}^{0,fcc}$, as discussed in Ref. [11].

However, in the COST507 database [5], the original assesment [4] was revised and the ε phase was modeled as HCP (A3) whereas the terminal η phase was modeled as separate "HCP_Zn" phase. This treatment is disapproved because it produces artifacts and inconsistency in Mg–Zn and Cd–Mg based systems [11]. These problems also occur in the assessments of Refs. [8,9] which are based on the COST507 version [5] from which the η phase model as "HCP_Zn" was taken.

3.3. The γ phase

The γ phase, defining the prototype of Cu_5Zn_8, is cI52 structure in the space group of *I-43m* [52]. The structure of the γ phase may be described for half the number of atoms in the cI52 unit cell by arranging two 26-atom clusters to form the Bcc (cI2) structure. The 26 atoms in the cluster are distributed over 4 vertices of an inner tetrahedron (IT), 4 vertices of an outer tetrahedron (OT), 6 vertices of an octahedron (OH) and 12 vertices of a cubo-octahedron (CO). Heidenstam et al. [53] and Gourdon et al. [54] investigated the distribution of the Cu and Zn atoms over all sites by using neutron diffraction. The three possible models, A, B, and C, proposed for atomic distribution over these sites (IT 4, OT 4, OH 6, CO 12) are shown in Table 3. The first model (A) is the distribution according to ideal stoichiometric Cu_5Zn_8 phase. Heidenstam et al. [53] reported that both models (B) and (C) are possible for site occupations. Occupation model B was accepted by Ref. [4] because it shows narrower maximum composition range compared to distribution C. However, the more recent diffraction results in Ref. [54] suggest the distribution (C) to be best. Therefore, if only the crystal structure information is considered, then the best

Table 3
Atomic distribution models and their constrained composition range for the γ phase.

Model[a]	Composition range (at% Zn)	IT 4 (8c)[b]	OT 4 (8c)	OH 6 (12e)	CO 12 (24 g)	References
A	61.54	Zn	Cu	Cu	Zn	[53,54]
B	46.15–76.92	(Cu,**Zn**)	(**Cu**,Zn)	Cu	Zn	[53]
C	15.38–84.62	Zn	Cu	(**Cu**,Zn)	(Cu,**Zn**)	[53,54]

[a] A=(**Zn**)4(**Cu**)4(**Cu**)6(**Zn**)12, B=(Cu,**Zn**)4(**Cu**,Zn)4(**Cu**)6(**Zn**)12, C=(**Zn**)4(**Cu**)4(**Cu**,Zn)6(Cu,**Zn**)12, the majority species are given in bold font.
[b] The Wyckoff notation (8c, 8c, 12e, 24g) for the 52 atoms unit cell is given in brackets.

sublattice model for the binary Cu–Zn γ phase should be (**Zn**)4(**Cu**)4(**Cu**,Zn)6(Cu,**Zn**)12, with major species highlighted by bold font. However, the extension into the Al–Cu–Zn ternary system needs additional considerations because the γ phases in the Cu–Zn and Cu–Al binary systems unite in complete solid solubility range. The atom distribution of the disordered γ phase in the Al–Cu binary system is (Al,Cu)4(**Cu**)4(**Cu**)6(Al,Cu)12 [55]. Both Al and Cu atom occupations in the first and fourth sublattices are near 50%, and randomly distributed. However, for the ordered γ-Cu_9Al_4 phase, the site occupations of Al and Cu in the first and fourth sublattices is not random any more. More detail will be discussed in Part II of this series, the paper on the Al–Cu binary system. Combined with the best model (C) in the Cu–Zn system, the model for the ternary Al–Cu–Zn γ phase should be (Al,Cu,Zn)4(**Cu**)4(**Cu**,Zn)6(Al,Cu,Zn)12. That model option was also recommended in Ref. [56] and discussed in the 1997 Ringberg workshop [57]. Although this model reflects the crystal structure of the γ phase perfectly, it was not applied in any published thermodynamic description because of its complexity; it involves $3\times2\times3=18$ end member parameters, not counting possible interaction parameters. We suggest to combine the two (Al,Cu, and Zn) sublattices and simplified it to (**Cu**)4(**Cu**,Zn)6(Al,Cu,Zn)16, which only contains 6 end members. That reduces to (**Cu**)4(**Cu**,Zn)6(Cu,**Zn**)16 for the Cu–Zn binary system containing 4 end members. Note that in this three-sublattice simplification Cu on the (Cu,**Zn**)16 sublattice is not a major species in the Cu–Zn binary system as opposed to the (Al,Cu,Zn)16 sublattice in the ternary system for Zn-poor compositions.

The Gibbs energy for the γ phase, (**Cu**)4(**Cu**,Zn)6(Cu,**Zn**)16, is described by the Compound-Energy Formalism [58] which reduces for this case of mixing on only 2 sublattices to:

$$G^{\gamma}=\sum_{i,j}y_i^{II}\cdot y_j^{III}\cdot G^{0,\gamma}_{Cu:i:j}+6RT\sum_i y_i^{II}\ln y_i^{II}+16RT\sum_j y_j^{III}\ln y_j^{III}+G^{ex,\gamma} \quad (3)$$

where y_i^{II} (y_j^{III}) is the site fraction of elemental constituents (i), (j) on the sublattice II (III), $G^{0,\gamma}_{Cu:i:j}$ is the Gibbs energy offormation of the endmember of the γ phase (per mol of formula unit). $G^{ex,\gamma}$ is the excess Gibbs energy and set to zero in this work.

3.4. Transition of the disordered phase β (Bcc) to the ordered phase β′ (Bcc_B2)

The disordered Bcc (A2) β phase is treated as substitutional solution phase, (Cu,Zn)1, and its Gibbs energy, G^{β}, is described by Eq. (2). The ordering of the β′ (B2) phase requires distinction of two sublattices with half the size, for edge and center atoms, in the sublattice model (Cu,Zn)0.5(Cu,Zn)0.5 to maintain the number of atoms given by the β phase, (Cu,Zn)1. Both phases, β and β′, are described by the same Gibbs energy function of β′, $G^{\beta'}$, which is constructed to produce the same values as G^{β} for the disordered state but different values for the ordered state following the works of Ansara et al. [59,60] and the book [61].

A unique function representing the Gibbs energy is used to describe the thermodynamic properties of both phases as follows:

$$G^{\beta'}=G^{\beta}(x_i)+G^{ord,B2}(y_i^I,y_i^{II})-G^{ord,B2}(y_i^I=x_i,y_i^{II}=x_i) \quad (4)$$

$$G^{ord,B2}(y_i^I,y_i^{II})=\sum_i\sum_{j\neq i}y_i^I y_j^{II}G^{0,ord,B2}_{i:j}+0.5RT\left(\sum_i y_i^I\ln y_i^I+\sum_i y_i^{II}\ln y_i^{II}\right)+G^{ex,B2} \quad (5)$$

$$G^{ex,B2}=y_{Cu}^I y_{Zn}^I\sum_i y_i^{II}L^{0,ord,B2}_{Cu,Zn:i}+y_{Cu}^{II}y_{Zn}^{II}\sum_i y_i^I L^{0,ord,B2}_{i:Cu,Zn} \quad (6)$$

The superscript *I* and *II* in these equations represent the first and second sublattice respectively; x_i (x_j) and y_i (y_j) are the molar fraction of element (i) (j) in the phase and its site fraction in the sublattice, respectively, with (i) (j)=Cu and Zn. The function-difference $G^{ord,B2}(y_i^I,y_i^{II})-G^{ord,B2}(y_i^I=x_i,y_i^{II}=x_i)$, or $\Delta G^{ord,B2}$, represents the change in the Gibbs energy of β due to ordering, thus forming the B2-phase β′. The disordered state, where site fractions become identical to molar fractions, $y_i^I=x_i, y_i^{II}=x_i$, results in $\Delta G^{ord,B2}=0$, thus $G^{\beta'}=G^{\beta}(x_i)$ as in Eq. (2).

The sum of the first and last terms in Eq. (5), $\sum_i\sum_{j\neq i}y_i^I y_j^{II}G^{0,ord,B2}_{i:j}+G^{ex,B2}$, equals $\Delta G_m^{\bullet}(y_i^I,y_i^{II})$ in the notation of Dupin and Ansara [60]. For the present choice of parameters we have $\Delta G_m^{\bullet}(y_i^I=x_i,y_i^{II}=x_i)=0$. Following a Thermo-calc newsletter by Sundman from 1991, the first appearance of these equations in published literature is found in Ref. [59]. However, in the double summation of Eq. (5) the exclusion $j\neq i$ is not given in Ref. [59], thus a parameter $G^{0,ord,B2}_{i:i}$may occur. The exclusion $j\neq i$ is explicitly only given in Ref. [60] where the equations are set up differently with the entropy part in Eq. (5) taken out to define $\Delta G_m^{\bullet}$. In fact, it is mandatory to set $G^{0,ord,B2}_{Cu:Cu}=G^{0,ord,B2}_{Zn:Zn}=0$ in order to comply with the general proper set of Eqs. (4)–(6) because current software packages do not automatically exclude $j\neq i$ in the summation. The advantage of writing the order/disorder model equations in the way of Eqs. (4)–(6) is that it makes clear that the parameters of the disordered phase may be chosen without any constraint for $G^{\beta}(x_i)$ as given in Table 4. Additional relations [59,60] only apply to the parameters of $G^{ord,B2}$ in Eqs. (5) and (6) to enable disordering by obtaining $\Delta G^{ord,B2}=0$ from the internal Gibbs energy minimization of $G^{\beta'}$at high temperature. These relations are observed by the additional parameters given for β′ in Table 4.

The ordering contribution to the excess Gibbs energy in Eq. (6) is written in the most simple way, as required for the β′ phase of Cu–Zn, where the parameters $L^{0,ord,B2}_{Cu,Zn:i}$ and $L^{0,ord,B2}_{i:Cu,Zn}$ are the zeroth order of the formal Redlich–Kister parameters that may be extended to higher order [59,60].

3.5. Parameter optimization

The thermodynamic description of Ref. [4] was used as a start point. First, the δ phase is introduced and the parameters of δ are optimized based on the relevant phase equilibrium data. Then the γ phase is replaced by the new model. Subsequently the parameters of other phases are optimized based on all the experimental phase equilibrium and thermodynamic data. At the last step, all the experimental data with properly adjusted weight are selected and all the parameters are optimized in fine tuning to obtain the final set of thermodynamic parameters. Thermodynamic calculations and the parameter optimization are performed using the Pandat software package (www.computherm.com) with PanOptimizer [62]. All thermodynamic Gibbs energy parameters determined in the present work are given in Table 4 and as supplementary file in electronic form for the Cu–Zn system (TDB).

Table 4
Phase names; name in tdb-parameters; models (sublattice formula), and parameters of the Gibbs energy equations developed in present work. Gibbs energy is given in J mol-formula^{-1} and temperature (T) is given in Kelvin. The Gibbs energies for the pure elements are found in the SGTE compilation [49].

Liquid; Liq; $(Cu,Zn)_1$
$L^{0,Liq}_{Cu,Zn} = -40688.6+12.8655\times T$
$L^{1,Liq}_{Cu,Zn} = 2252.3-4.8069\times T$
$L^{2,Liq}_{Cu,Zn} = 5405.9-2.9197\times T$

α, (Cu); Fcc; $(Cu,Zn)_1$
$L^{0,Fcc}_{Cu,Zn} = -40{,}716+8.3\times T$
$L^{1,Fcc}_{Cu,Zn} = +4812.8-4\times T$

η, (Zn); Hcp; $(Cu,Zn)_1$
$L^{0,Hcp}_{Cu,Zn} = -15492.5-12.276\times T$

β; Bcc; $(Cu,Zn)_1$
$L^{0,Bcc}_{Cu,Zn} = -48{,}042+9.97\times T$
$L^{1,Bcc}_{Cu,Zn} = 6100-6\times T$
$L^{2,Bcc}_{Cu,Zn} = 1000$

β′; Bcc_B2; $(Cu,Zn)_{0.5}(Cu,Zn)_{0.5}$
$G^{ord,B2}_{Cu:Cu} = G^{ord,B2}_{Zn:Zn} = 0$
$G^{ord,B2}_{Cu:Zn} = G^{ord,B2}_{Zn:Cu} = -3075$
$L^{0,ord,B2}_{Cu:Cu,Zn} = L^{0,ord,B2}_{Zn:Cu,Zn} = L^{0,ord,B2}_{Cu,Zn:Cu} = L^{0,ord,B2}_{Cu,Zn:Zn} = 3075$

γ; Gamma; $(Cu)_4(\mathbf{Cu},Zn)_6(Cu,\mathbf{Zn})_{16}$
$G^{0,Gamma}_{Cu:Cu:Cu} = 2600+26\times G^{0,Fcc}_{Cu}$
$G^{0,Gamma}_{Cu:Cu:Zn} = -284{,}704-59.332\times T+10\times G^{0,Fcc}_{Cu}+16\times G^{0,Hcp}_{Zn}$
$G^{0,Gamma}_{Cu:Zn:Cu} = 20\times G^{0,Fcc}_{Cu}+6\times G^{0,Hcp}_{Zn}$
$G^{0,Gamma}_{Cu:Zn:Zn} = -62{,}316-112.4872\times T+4\times G^{0,Fcc}_{Cu}+22\times G^{0,Hcp}_{Zn}$

δ; Delta; $(Cu,Zn)_1$
$G^{0,Delta}_{Zn} = 4375.32-2.955\times T+G^{0,Hcp}_{Zn} = 1488.36-0.4446\times T+G^{0,Bcc}_{Zn}$
$G^{0,Delta}_{Cu} = 5727.15-1.6807\times T+G^{0,Fcc}_{Cu} = 1710.15-0.4257\times T+G^{0,Bcc}_{Cu}$
$L^{0,Delta}_{Cu,Zn} = -54593.9+12.8111\times T$
$L^{1,Delta}_{Cu,Zn} = 142+6.0249\times T$

ε; Eps; $(Cu,Zn)_1$
$G^{0,Eps}_{Cu} = G^{0,Hcp}_{Cu}$
$G^{0,Eps}_{Zn} = G^{0,Fcc}_{Zn}$
$L^{0,Eps}_{Cu,Zn} = -36818.3+6{,}5\times T$
$L^{1,Eps}_{Cu,Zn} = 27160.5-10.8351\times T$

4. Results and discussion

4.1. Phase diagram

The "experimental" phase diagram is taken from the most recent and most comprehensive critical review performed by Miodownik [10]. No additional, more recent experimental phase equilibrium data could be found except the EMF measurement results in Ref. [7]. Fig. 1 represents the calculated phase diagrams of Cu–Zn system in this work and Ref. [4] compared with the experimental phase diagram [10]. For better readability, "original" data points are not shown here, the reader is referred to Ref. [10]. The calculated phase diagram by Ref. [4] agrees with the assessed phase diagram [10] very well. The later published thermodynamic descriptions [7,8,9] did not show improved phase diagram description, and some of them are even worse compared to Ref. [4]. Thus, only the calculated phase diagram by Ref. [4] is shown for comparison to enhance readability. A complete comparison of the previous Calphad-type descriptions [4,7–9] with the present work and the experimentally assessed basis [10] is given for the

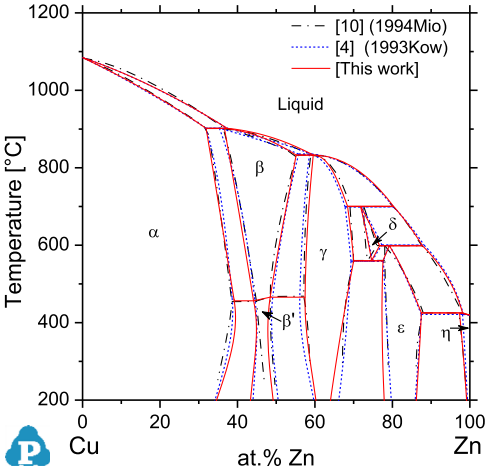

Fig. 1. Phase diagram of Cu–Zn system calculated in this work compared with the experimentally assessed one [10] and the calculated one by Ref. [4]. Additional shorthand-notation for references, indicating year and first author, is provided in brackets.

invariant reactions in Table 5. Compared with the experimental data [10], the presently calculated phase diagram and invariant reactions show some improvement in the δ phase region and Zn-rich corner from the basic work of Ref. [4], while keeping the same level of agreement in the rest of the phase diagram.

The improved description of the phase equilibria for the Zn-rich corner was accomplished by careful examination of all original experimental data for Zn-rich alloys. David et al. [7] measured μ_{Zn} by EMF of Zn–Cu alloys with 90–98 at% Zn, which is the most recent experimental work at Zn-rich corner. The measured EMF data converted to relative chemical potential and compared with calculated results are shown in Fig. 2. Pure Zn was used as reference electrode in the EMF measurement, which melts at 419.6 °C. At that temperature the reference state changes and the measured open circuit voltage, $E°$, converts to the chemical potential difference as follows:

$$-2FE° = \mu_{Zn} - G^{0,Liquid}_{Zn}(T > 419.6°C) \quad (7a)$$

$$-2FE° = \mu_{Zn} - G^{0,Hcp}_{Zn}(T < 419.6°C) \quad (7b)$$

where F is Faraday's constant and the factor 2 reflects the Zn^{2+} ions. Thus, the calculated curves for all alloys in Fig. 2 show a kink at 419.6 °C, even changing sign of the slope. There can be no discontinuity in any of these curves. The second kink, observed for all studied alloys, is at 425 °C, the temperature of the peritectic equilibrium liquid+ε=(Zn). Only the curve for the alloy with 98 at% Zn shows a third kink between these temperatures, at 424 °C, the (Zn)+liquid/(Zn) phase boundary. That curve even shows a fourth kink at 352 °C, the (Zn)/ε+(Zn) phase boundary, where it joins the calculated curves for all other alloys at lower temperature. All these curves also overlap above the peritectic at 425 °C in the ε+liquid region up to the respective liquidus temperatures where the curves bend to the single phase region of liquid.

The calculated results are in reasonable agreement with the experimentally measured values at high Zn content (96 and 98 at% Zn), while slightly deviating from the experimental data with Zn content less than 96 at% Zn at the high temperature end of 500–550 °C. However, the trend of these experimental data with the kink at the ε+liquid/liquid phase boundary is not consistent with the experimental liquidus data from other sources [10,43,44] with decreasing Zn content and higher temperature.

Fig. 3 shows the calculated phase diagrams of Cu–Zn at Zn-rich

Table 5
Comparison of calculated and experimental invariant reactions in the Cu–Zn system.

Reaction	Temperature (°C)						Phase	Composition (at% Zn)					
	(1)	(2)	(3)	(4)	(5)	(6)		(1)	(2)	(3)	(4)	(5)	(6)
α+L↔β	902	**902**	903	902	900	903	L	36.8	**37.3**	37.3	37.2	–	38.4
							α	31.9	**31.9**	31.9	31.9	–	32.7
							β	36.1	**36.0**	35.3	35.1	35.8	36.1
β+L↔γ	834	**833**	835	837	834	835	L	59.1	**59.6**	59.2	60.6	–	59.2
							β	55.8	**55.1**	55.8	57.2	–	55.4
							γ	59.1	**59.6**	58.6	59.9	58.7	59.1
γ+L↔δ	700	**700**	700	700	703	699	L	79.8	**80.3**	80.2	82.0	–	80.1
							γ	69.2	**68.4**	67.8	68.9	–	66.9
							δ	72.5	**71.8**	71.9	72.5	72.0	72.0
δ+L↔ε	598	**598**	600	599	600	599	L	87.9	**87.8**	88.2	89.2	–	88.1
							δ	76.0	**76.7**	77.3	77.3	–	77.5
							ε	78.0	**79.2**	79.2	79.5	79.2	79.3
δ↔γ+ε	560	**560**	559	560	559	561	δ	73.5	**74.6**	74.9	74.3	74.9	75.1
							γ	70.0	**70.0**	69.3	69.0	–	68.7
							ε	78.0	**77.6**	77.7	77.6	–	77.8
ε+L↔η	425	**425**	422	425	419	421	L	98.3	**98.2**	98.3	98.35	–	98.2
							ε	88.0	**87.5**	87.5	87.4	–	87.4
							η	97.2	**97.3**	98.1	97.6	98.3	98.1
Ordering reaction													
β↔β′, γ	468	**466**	–	–	–	–	γ	57.0	**57.5**	–	–	–	–
							β	48.2	**48.4**	–	–	–	–
β↔β′, α	454	**456**	–	–	–	–	β	44.8	**44.2**	–	–	–	–
							α	38.27	**39.2**	–	–	–	–

(1) Assessed Ref. [10]; (2) calculated [this work], bold font; (3) calculated Ref. [4]
(4) calculated Ref. [7]; (5) calculated "full description" Ref. [8]; (6) calculated Ref. [9].

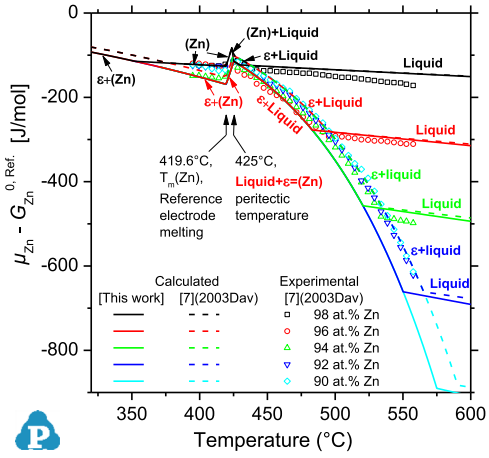

Fig. 2. Chemical potential of Zn in Zn-rich Cu–Zn alloys. Symbols: EMF experimental data [7]; dashed lines: calculated values in Ref. [7]; solid lines: calculated values in this work. Reference state changes from liquid Zn for $T > 419.6$ °C to solid Zn (Hcp) for $T < 419.6$ °C.

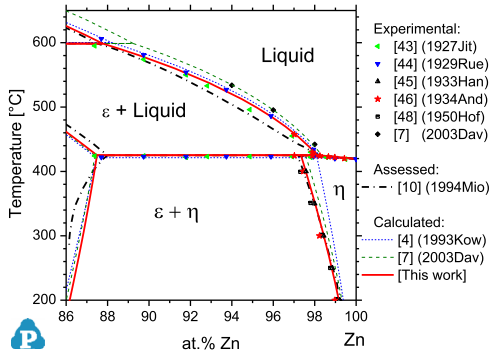

Fig. 3. Zn-rich part of the Cu–Zn phase diagram; comparison to previous calculations [4,7], experimental assessment [10] and original experimental data [7,43–48].

corner together with all other original experimental results [7,43–48]. The calculation by Ref. [7] apparently only considered their own EMF results, the liquidus data of the three alloys at 94, 96, and 98 at% Zn [7] are exactly reproduced. The calculated liquidus line [7] is slightly above other experimental data of Zn-rich alloys in that range, but the deviation increases drastically for more Cu-rich alloys. In the composition range with less than 94 at% Zn the calculated liquidus [7] is unacceptably high and it is also worse than [4] in the other parts of the phase diagram, for example the β and γ phase boundaries.

The calculated liquidus line of the present work is somewhat above the liquidus in the review of Ref. [10] but agrees well with the original experimental data. The solid solubility of Cu in the η phase calculated by Ref. [4] is much too low around 300–425 °C and the present modeling provides significant improvement. The original experimental data on the L+ε↔η peritectic reaction are collected in Table 6 [39–47] and compared to the review [10] and the calculations from this work and [4]. Miodownik [10] mainly accepted the work of Anderson et al. [46] who carried out dedicated experimental work to determine the solid solubility of Cu in η phase and the peritectic through thermal analysis, quench

Table 6
Detailed data on the Zn-rich peritectic reaction $\varepsilon + L \leftrightarrow \eta$, see also Fig. 3. All original experimental data are compared with the present work and the benchmark assessment of Kowalski and Spencer [4].

Temperature (°C)	Cu content in phases (at%)			Reference
	ε	L	η	
425				[39] Cited in Ref. [46]
425	13		3.1	[40] Cited in Ref. [46]
426				[42]
423	12.5	1.54	2.1	[41]
423	13		2.1	[43]
423				[44]
424			2.7	[45]
425		1.9	2.8	[46]
424				[47]
425	12	1.8	2.8	[10]
425	**12.5**	**1.8**	**2.7**	**[This work]**
422	12.5	1.7	1.9	[4]

experiments, X-ray, microstructure observation and electrical conductivity measurement. The presently calculated peritectic temperature of 425 °C is the same as that assessed temperature [10], another improvement compared to the value of 422 °C calculated by Ref. [4].

4.2. Thermodynamic properties of the liquid phase

Fig. 4 shows the reported experimental data [17–19,31,32] for the enthalpy of mixing of the liquid phase. Although five sets of enthalpy data were reported [17–19,31,32], actually, only two of them [17,18] were directly measured by calorimetry. The enthalpy of mixing data at 1000 °C in Ref. [19] were recalculated from their measured enthalpy of formation of solid phases at 20 °C. The reported enthalpy of mixing data at 775 °C were derived from the temperature dependence of measured vapor pressure of Zn over liquid phase from 700 to 850 °C [32]. Similarly, the values at 900 °C were derived from the EMF results of μ_{Zn} from 800 to 900 °C [31]. The vapor pressure and EMF results will be directly compared with calculated chemical potential, μ_{Zn}, later; the derived integral enthalpy data [19,31,32], shown by open symbols in Fig. 4, must be disregarded following the true Calphad spirit.

Gierlotka and Chen [8] have chosen the derived data from Refs. [19,31,32] as basis for modeling the liquid enthalpy of mixing, assuming a strong temperature dependence, as exemplified by their calculated results at 775 and 1100 °C in Fig. 4. A similar

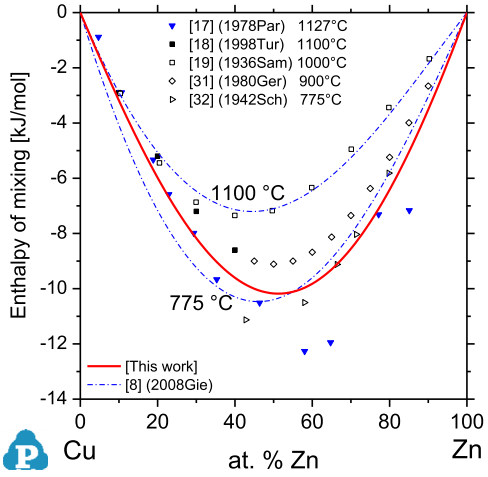

Fig. 4. Calculated enthalpy of mixing of the liquid phase compared with experimental data, solid symbols for direct experimental data [17,18] and open symbols for derived data [19,31,32]. Reference states: pure liquid elements.

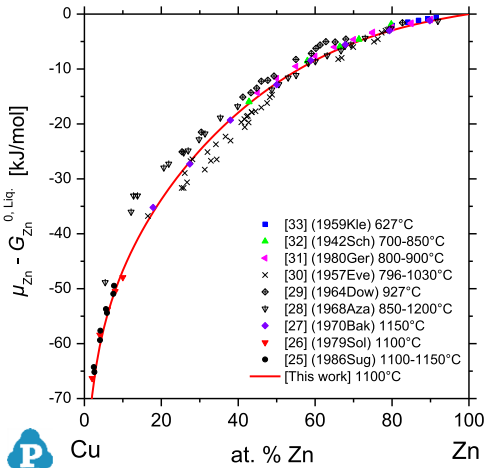

Fig. 5. Chemical potential of Zn in liquid phase, comparison of experimental data [25–32] with calculated results of this work at 1100 °C. Reference state is liquid Zn.

scheme was followed by Wang et al. [9], using the derived data [19,31,32] for an assumed temperature dependence of the liquid mixing enthalpy; their calculated results [9] are not shown here to enhance readability of the diagram. Both sets of calculated enthalpies deviate significantly from the direct experimental data [17,18] shown by solid symbols in Fig. 4.

Considering the scatter of the direct experimental data [17,18], any temperature dependence in modeling the enthalpy is not justified. The calculated temperature independent results in this work show reasonable agreement with the experimental data. The two data points at Zn=58 at% and 65 at% reported by Ref. [17] are considered questionable, they even fall out of the range of experimental data from same author at other compositions.

Fig. 5 represents the calculated chemical potential of Zn in liquid at 1100 °C in agreement with experimental data from Refs. [25–32]. The Zn-rich side from 40 to 100 at% Zn is shown in Fig. 6 with focus on the temperature dependence of the chemical potential. The experimental chemical potential results vary only little in the wide temperature range from 627 °C to 1200 °C. The calculated results at 627 °C agree well with experimental data [33]. The chemical potential measured by Refs. [31,32] from 700 °C to 900 °C show good agreement with our calculated values at 850 °C. The good agreement between the calculated and experimental chemical potential data, within the experimental scatter, is another confirmation that the assumption of strong temperature

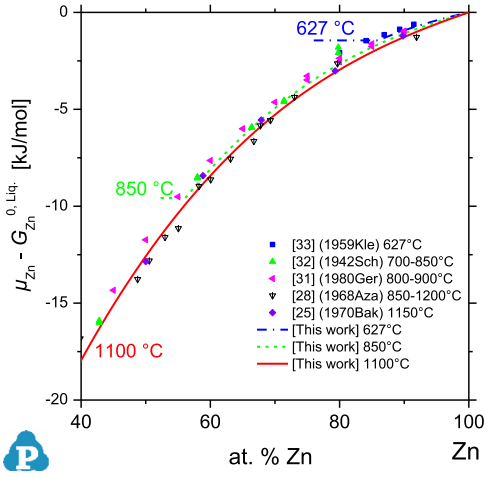

Fig. 6. Chemical potential of Zn in Zn-rich liquid phase, comparison of experimental data [25,28,31–33] with calculated results of this work at different temperatures. Reference state is liquid Zn.

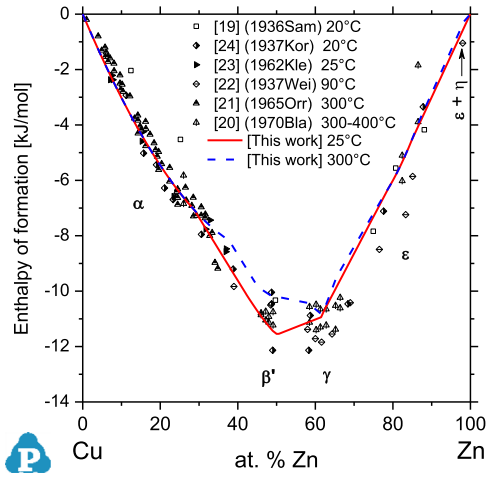

Fig. 7. Enthalpy of formation of the solid phases obtained from experimental data [19–24] compared with presently calculated values at 25 °C and 300 °C. Reference states are solid Cu (Fcc) and Zn (Hcp).

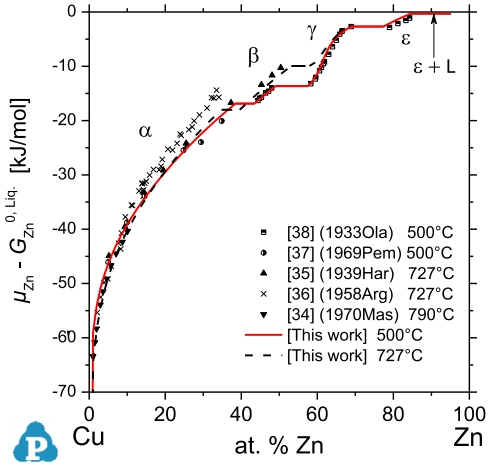

Fig. 8. Chemical potential of Zn for solid phases from experimental data [34–38] compared with presently calculated values at 500 °C and 727 °C. Reference state is liquid Zn.

dependence of liquid enthalpy of mixing following the derived enthalpy values [31,32] is not reasonable.

4.3. Thermodynamic properties of solid phases

Fig. 7 compares the calculated enthalpy of formation of the solid phases at 25 °C and 300 °C with the experimental data. The calculated results agree well with the experimental data, and the ordered β′ (Bcc_B2) phase show strong temperature dependence of the enthalpy value. The calculated chemical potential of Zn for solid phases also agrees with the experimental data at 500 °C and 727 °C as shown in Fig. 8. The experimental data of Ref. [36] around 20–40 at% Zn are inconsistent with other experimental data in that range and not accepted in the present work. Compared to the assessment of Kowalski and Spencer [4], the present work uses a smaller number of adjustable interaction parameters. The third-order parameter $L^{2,Fcc}_{Cu,Zn}$ is not used at all and $L^{2,Bcc}_{Cu,Zn}$ is simplified to be temperature independent. Calculated site fractions of the major constituents in the γ phase at constant composition of 62 at% Zn show decreasing values with increasing temperature. Values of $y^{(II)}_{Cu} = 0.88$ and $y^{(III)}_{Zn} = 0.96$ at 824 °C are attained, where liquid starts appearing. This is in accordance with our selection and indication of major species in the second and third sublattice, (**Cu**)4(**Cu**,Zn)6(Cu,**Zn**)16. However, there are no experimental data to compare with.

5. Conclusion

The key improvements of this thermodynamic re-assessment from previous descriptions are:

(1) The quantitative description of Zn-rich phase equilibria and thermodynamic data is provided without sacrificing the quality of description in the full composition range.
(2) The hexagonal structure of δ phase is acknowledged by modeling it as separate phase from Bcc.
(3) The γ phase is modeled as a three sublattice model which reflects the crystal structure of the phase in a simplification allowing extension to ternary systems.
(4) The liquid enthalpy of mixing is modeled as temperature independent, disapproving the previously assumed temperature dependence based on derived enthalpy data.

Acknowledgment

This study is supported by the German Research Foundation (DFG) under Grant no. Schm 588/41. We would like to acknowledge fruitful discussions with Nathalie Dupin and Bo Sundman on the Bcc A2/B2 modeling.

Appendix A. Supplementary material

Supplementary data associated with this article can be found in the online version at http://dx.doi.org/10.1016/j.calphad.2015.09.010.

References

[1] G.O. Cowie, Zinc Alloy Castings: Product Design and Development, International Lead Zinc Research Organization, Inc, Research Triangle Park, North Carolina, 1992.
[2] N. Kang, H.S. Na, S.J. Kim, C.Y. Kang, Alloy design of Zn–Al–Cu solder for ultra high temperatures, J. Alloy. Compd. 467 (2009) 246–250.
[3] P.J. Spencer, A thermodynamic evaluation of the Cu–Zn system, Calphad 10 (1986) 175–185.
[4] M. Kowalski, P.J. Spencer, Thermodynamic reevaluation of the Cu–Zn system, J. Ph. Equilib. 14 (1993) 432–438.
[5] M. Kowalski, P.J. Spencer, System Cu–Zn, in: I. Ansara, A.T. Dinsdale, M.H. Rand (Eds.), COST 507: Thermochemical Database for Light Metal Alloys. Definition of Thermodynamical and Thermophysical Properties to Provide a Database for the Development of New Light Alloys, vol. 2, European Commission, Brussels, Belgium, 1998, pp. 186–191.
[6] H. Liang, Y.A. Chang, A thermodynamic description for the Al–Cu–Zn system, J. Ph. Equilib. 19 (1998) 25–37.
[7] N. David, J.M. Fiorani, M. Vilasi, J. Hertz, Thermodynamic reevaluation of the Cu–Zn system by electromotive force measurements in the zinc-rich part, J. Ph. Equilib. 24 (2003) 240–248.
[8] W. Gierlotka, S.W. Chen, Thermodynamic descriptions of the Cu–Zn system, J. Mater. Res. 23 (2008) 258–263.
[9] J. Wang, H. Xu, S. Shang, L. Zhang, Y. Du, W. Zhang, S. Liu, P. Wang, Z.-K. Liu, Experimental investigation and thermodynamic modeling of the Cu–Si–Zn system with the refined description for the Cu–Zn system, Calphad 35 (2011) 191–203.
[10] A.P. Miodownik, Cu–Zn (copper–zinc), in: D.E. Laughlin, D.J. Chakrabarti, P. R. Subramanian (Eds.), Phase Diagrams of Binary Copper Alloys, ASM International, Materials Park, OH, 1994, pp. 487–496.
[11] R. Schmid-Fetzer, B. Hallstedt, Is zinc HCP_ZN or HCP_A3? Calphad 37 (2012) 34–36.
[12] N. Saunders, System Al–Cu, in: I. Ansara, A.T. Dinsdale, M.H. Rand (Eds.), COST 507: Thermochemical Database for Light Metal Alloys. Definition of Thermodynamical and Thermophysical Properties to Provide a Database for the Development of New Light Alloys, vol. 2, European Commission, Brussels, Belgium, 1998, pp. 28–33.
[13] E.A. Owen, L. Pickup, The relation between mean atomic volume and composition in copper–zinc alloys, Proc. R. Soc. Lond. A 140 (1933) 179–191.

[14] T.B. Massalski, H.W. King, The lattice spacing relationships in H.C.P. ϵ and η phases in the systems Cu–Zn, Ag–Zn; Au–Zn and Ag–Cd, Acta Metall. 10 (1962) 1171–1181.
[15] K. Schubert, E. Wall, Zur Kristallstruktur der δ-Hochtemperaturphase des Systems Kupfer-Zink, Z. Metallkd. 40 (1949) 383–385.
[16] J. Lenz, K. Schubert, Über einige Leerstellen- und Stapelvarianten der Beta-Messing Strukturfamilie, Z. Metallkd. 62 (1971) 810–816.
[17] K. Parameswaran, G. Healy, A calorimetric investigation of the copper-zinc system, Metall. Trans. B 9 (1978) 657–664.
[18] M.A. Turchanin, Enthalpies of formation of liquid copper alloys with 3d transition metals, Russ. Metall. (1998) 29–38.
[19] H.-O.V. Samson-Himmelstjema, Die Wärmeinhalte und Bildungswärmen geschmolzener Legierungen, Z. Metallkd. 28 (1936) 197–202.
[20] G.R. Blair, D.B. Downie, A calorimetric study of silver–zinc and copper–zinc alloys, Met. Sci. 4 (1970) 1–5.
[21] R.L. Orr, B.B. Argent, Heats of formation of the alpha-brasses, Trans. Faraday Soc. 61 (1965) 2126–2131.
[22] F. Weibke, Beiträge zur systematischen Verwandtschaftslehre. 71. Über die Bildungswärmen im System Kupfer-Zink, Z. Anorg. Allg. Chem. 232 (1937) 289–296.
[23] O.J. Kleppa, R.C. King, Heat of formation of the solid solutions of zinc, gallium and germanium in copper, Acta Metall. 10 (1962) 1183–1186.
[24] F. Körber, W. Oelsen, Zur Thermochemie der Legierungen III: Die Bildungswärmen der Zweistofflegierungen Eisen–Antimon, Kobalt–Antimon, Nickel–Antimon, Kobalt–Zinn, Nickel–Zinn, Kupfer–Zinn und Kupfer–Zink für den Gußzustand, Mitteilungen aus dem Kaiser-Wilhelm-Institut für Eisenforschung zu Düsseldorf (1937), p. 209–219.
[25] E.H. Baker, Vapor pressures and thermodynamic behavior of liquid zinc–copper alloys at 1150 °C, Trans. Inst. Min. Met. Sect. C 79 (1970) C1–C5.
[26] S. Sugino, H. Hagiwara, Activity of zinc in molten copper and copper–gold alloys, J. Jpn. Inst. Met. 50 (1986) 186–192.
[27] S.L. Solovev, M.V. Knyazev, Y.I. Ivanov, A.V. Vanyukov, Mass spectrometric study of the partial characteristics of zinc in a copper–zinc system, Mosc. Inst. Steel Alloy. 45 (1979) 841–844.
[28] T. Azakami, A. Yazawa, Activities of zinc and cadmium in liquid copper base alloys: thermodynamic studies of liquid copper alloys (3rd report), J. Min. Metall. Inst. Jpn. 84 (1968) 1663–1668.
[29] D.B. Downie, Thermodynamic and structural properties of liquid zinc/copper alloys, Acta Metall. 12 (1964) 875–882.
[30] L.H. Everett, P.W.M. Jacobs, J.A. Kitchener, The activity of zinc in liquid copper–zinc alloys, Acta Metall. 5 (1957) 281–284.
[31] U. Gerling, B. Predel, On the thermodynamic properties of liquid copper–zinc-alloys, Z. Metallkd. 71 (1980) 158–164.
[32] A. Schneider, H. Schmid, Die Dampfdrucke des Zinks und Cadmiums über ihren binären flüssigen Legierungen mit Kupfer, Silber und Gold. Metalldampfdrucke III, Z. Elektrochem. 48 (1942) 627–639.
[33] O.J. Kleppa, C.E. Thalmayer, An E.M.F. investigation of binary liquid alloys rich in zinc, J. Phys. Chem. 63 (1959) 1953–1958.
[34] D.B. Masson, J.-L. Sheu, Variations in the composition dependence of the activity coefficient in terminal solid solutions of Ag−Zn, Ag−Cd, and Cu−Zn, Metall. Trans. 1 (1970) 3005–3009.
[35] R. Hargreaves, The vapour pressure of zinc in brasses, J. Inst. Met. 64 (1939) 115–125.
[36] B.B. Argent, D.W. Wakeman, Thermodynamic properties of solid solutions. Part 1. Copper+zinc solid solution, Trans. Faraday Soc. 54 (1958) 799–806.
[37] J.P. Pemsler, E.J. Rapperport, Thermodynamic activity measurements using atomic absorption: copper–zinc, Trans. Met. Soc. AIME 245 (1969) 1395–1400.
[38] A. Olander, Eine elektrochemische untersuchung von Messing, Z. Phys. Chem. A164 (1933) 428–438.
[39] V.E. Tafel, Metallurgie, vol. 5 1908, pp. 343–352. 375–383, 413–30 (cited in Ref. [46]).
[40] N. Parravano, Gazz. Chim. Ital. (1914) 475–502 (cited in Ref. [46]).
[41] O. Bauer, M. Hansen, Der Aufbau der Kupfer-Zinklegierungen, Z. Metallkd. 19 (1927) 423–430.
[42] J.L. Haughton, K.E. Bingham, The constitution of the alloys of aluminium, copper, and zinc containing high percentages of zinc, Proc. R. Soc. Lond. A 99 (1921) 47–69.
[43] D. Jitsuka, Nachprüfung des Zustandschaubildes des Systems Kupfer-Zink, Z. Metallkd. 19 (1927) 396–403.
[44] R. Ruer, K. Kremers, Das System Kupfer–Zink, Z. Anorg. Allg. Chem. 184 (1929) 193–231.
[45] M. Hansen, W. Stenzel, The solubility of copper in zinc, Metallwirtschaft 12 (1933) 539–542.
[46] E.A. Anderson, M.L. Fuller, R.L. Wilcox, J.L. Rodda, The high-zinc region of the copper–zinc phase equilibrium diagram, Trans. AIME 111 (1934) 264–292.
[47] J. Schramm, Contribution to the Cu–Zn diagram, Metallwirtschaft 14 (1935) 995–1001.
[48] W. Hofmann, G. Fahrenhorst, Die Ausscheidungsgeschwindigkeit in Zink-Aluminium- und Zink-kupfer-Mischkristallen hohen Reinheitsgrades, Z. Metallkd. 41 (1950) 460–462.
[49] A.T. Dinsdale, SGTE data for pure elements, Calphad 15 (1991) 317–425.
[50] P. Villars, L.D. Calvert, Pearson's Handbook of Crystallographic Data for Intermetallic Phases, vol. 1, ASTM International, Ohio (1985), p. 529 , pp. 738.
[51] T. Massalski, J.L. Murray, L. Bennett, H. Baker, Binary alloy phase diagrams, American Society for Metals, Metals Park, Ohio (1986), p. 980.
[52] A.J. Bradley, C.H. Gregory IX, A comparison of the crystal structures of Cu_5Zn_8 and Cu_5Cd_8, Philos. Mag. 12 (1931) 143–162.
[53] O. von Heidenstam, A. Johansson, S. Westman, A redetermination of the distribution of atoms in Cu_5Zn_8, Cu_5Cd_8, and Cu_9Al_4, Acta Chem. Scand. 22 (1968) 653–661.
[54] O. Gourdon, D. Gout, D.J. Williams, T. Proffen, S. Hobbs, G.J. Miller, Atomic distributions in the γ-brass structure of the Cu−Zn system: a structural and theoretical study, Inorg. Chem. 46 (2007) 251–260.
[55] X.J. Liu, I. Ohnuma, R. Kainuma, K. Ishida, Phase equilibria in the Cu-rich portion of the Cu–Al binary system, J. Alloy. Compd. 264 (1998) 201–208.
[56] S.G. Fries, I. Hurtado, T. Jantzen, P.J. Spencer, K.C. Hari Kumar, F. Aldinger, P. Liang, H.L. Lukas, H.J. Seifert, Present achievements, problems and perspectives associated with a semi-empirical study of the Al–Cu–Mg–Si–Zn light alloy system, J. Alloy. Compd. 267 (1998) 90–99.
[57] I. Ansara, B. Burton, Q. Chen, M. Hillert, A. Fernandez-Guillermet, S.G. Fries, H. L. Lukas, H.-J. Seifert, W.A. Oates, Group 2: models for composition dependence, Calphad 24 (2000) 19–40.
[58] M. Hillert, The compound energy formalism, J. Alloy. Compd. 320 (2001) 161–176.
[59] I. Ansara, N. Dupin, B. Sundman, Reply to the paper: when is a compound energy not a compound energy? A critique of the 2-sublattice order/disorder model, Calphad 21 (1997) 535–542.
[60] N. Dupin, I. Ansara, On the sublattice formalism applied to the B2 phase, Z. Metallkd. 90 (1999) 76–85.
[61] H.L. Lukas, S.G. Fries, B. Sundman, Computational Thermodynamics: The Calphad Method, Cambridge University Press, Cambridge (2007), p. 141.
[62] W. Cao, S.L. Chen, F. Zhang, K. Wu, Y. Yang, Y.A. Chang, R. Schmid-Fetzer, W. A. Oates, PANDAT software with PanEngine, PanOptimizer and PanPrecipitation for multi-component phase diagram calculation and materials property simulation, Calphad 33 (2009) 328–342.